

RESEARCH ARTICLE

10.1002/2017JF004371

Key Points:

- A range of radial viscoelastic Earth profiles is applied to past and future Antarctic variations using a coupled ice sheet–Earth model
- Profiles with low mantle viscosity and thin lithosphere have significant negative feedbacks on ice retreat, on 10 to 10³ year timescales
- Coupled models with lateral variations may be needed to capture large contrasts in Earth properties between East and West Antarctica

Supporting Information:

- Supporting Information S1

Correspondence to:

D. Pollard,
pollard@essc.psu.edu

Citation:

Pollard, D., Gomez, N., & Deconto, R. M. (2017). Variations of the Antarctic ice sheet in a coupled ice sheet–Earth–sea level model: Sensitivity to viscoelastic Earth properties. *Journal of Geophysical Research: Earth Surface*, 122, 2124–2138. <https://doi.org/10.1002/2017JF004371>

Received 18 MAY 2017

Accepted 13 OCT 2017

Accepted article online 18 OCT 2017

Published online 7 NOV 2017

Variations of the Antarctic Ice Sheet in a Coupled Ice Sheet–Earth–Sea Level Model: Sensitivity to Viscoelastic Earth Properties

David Pollard¹, Natalya Gomez², and Robert M. Deconto³

¹Earth and Environmental Systems Institute, Pennsylvania State University, University Park, PA, USA, ²Department of Earth and Planetary Sciences, McGill University, Montreal, Quebec, Canada, ³Department of Geosciences, University of Massachusetts, Amherst, MA, USA

Abstract A coupled ice sheet–solid Earth–sea level model is applied to long-term variations of the Antarctic ice sheet. A set of radially varying viscoelastic profiles in the global Earth model is used to explore feedbacks on ice sheet variability, including one with a very weak upper mantle zone and thin lithosphere representative of West Antarctic regions. Simulations are performed for (1) the deglacial retreat over the last 20,000 years, (2) the future 5,000 years with greenhouse-gas scenario Representative Concentration Pathway 8.5 (RCP8.5), and (3) the warm Pliocene 3 Ma. For the deglacial period a large ensemble of 625 simulations is analyzed, with a score computed for each run based on comparisons to geologic and modern data. For each of the five Earth profiles, the top-scoring combinations of the other model parameters in the ensemble are used to perform future and Pliocene simulations. For the last deglacial retreat, the viscoelastic Earth profiles produce relatively small differences in overall ice volume and equivalent sea level. In contrast, profiles with weak upper mantle and thin lithosphere produce strong negative feedback and less ice retreat in the future and Pliocene runs. This is due to the faster pace of ice sheet retreat in these runs, leading to greater lags in the viscous bedrock rebound behind the unloading, which allows for greater influence of the viscosity profiles. However, the differences in grounding-line retreat are located primarily in East Antarctic basins, where a weak upper mantle and thin lithosphere may not be realistic, emphasizing the need for lateral heterogeneity in the Earth model.

1. Introduction

The deformation of bedrock topography below ice sheets has important feedbacks on long-term ice evolution, especially for marine sectors of Antarctica where ice fluxes across the grounding line are very sensitive to bathymetry (Feldmann & Levermann, 2015; Mercer, 1978; Schoof, 2007; Weertman, 1974). For instance, during ice sheet retreat the reduced ice load around the ice margin allows bedrock to rebound, shallowing the bathymetry and reducing ice flux across the grounding line. As a result, greater ice thicknesses are maintained upstream which slows grounding-line recession (Adhikari et al., 2014; Gomez et al., 2015, 2013; Konrad et al., 2015). Many long-term ice sheet modeling studies have used basic time-lagged bedrock relaxation toward isostasy, or simple ELRA (Elastic Lithosphere Relaxed Asthenosphere) models, but these greatly simplify asthenospheric flow (e.g., Le Meur & Huybrechts, 1996). Recent studies continue to use ELRA (e.g., Deconto & Pollard, 2016), or intermediate bed models with spatially varying flow in a viscous half-space below an elastic plate (Bueler et al., 2007; Golledge et al., 2015; Lingle & Clark, 1985).

Another approach in the study of long-term ice sheet evolution has been to adopt comprehensive global models of sea level change that include models of viscoelastic Earth deformation and rotational changes in response to surface (ice and water) loading, and gravitationally self-consistent changes in sea surface height. Prescribed vertical viscoelastic earth profiles and ice load histories that serve as inputs to a global Earth–sea level model may be tuned through comparisons of predicted sea level changes against local relative sea level records (e.g., Kendall et al., 2005; Lambeck et al., 1998; Mitrovica & Forte, 2004; Peltier, 2004; Stocchi et al., 2013; Whitehouse, Bentley, Milne et al., 2012). Relatively few studies have coupled dynamic ice sheet models interactively with this type of Earth model, either with sea level computed in post-processing (Briggs et al., 2013; Tarasov & Peltier, 2004) or within the coupled model (d. Adhikari et al., 2016; de Boer et al., 2014, 2017; Gomez et al., 2013, 2015; Konrad et al., 2015).

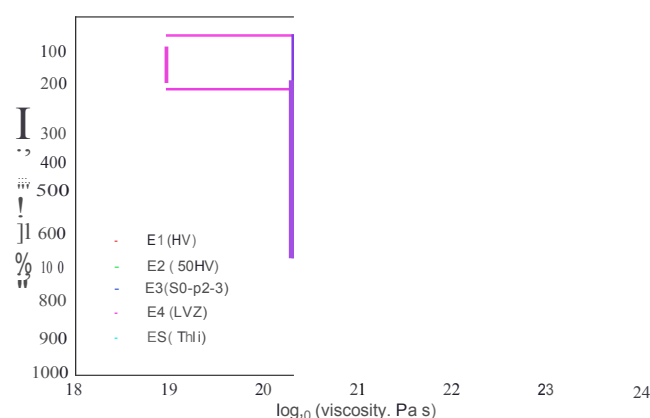


Figure 1. Viscosity versus depth for the five viscoelastic Earth profiles (E1 to E5) used in this study. E1: HV, high viscosity, representing a broad class of globally tuned Earth models. E2: 50 HV, thin lithosphere. E3: SO-p2-3, low viscosity upper mantle, thin lithosphere. E4: LVZ, very low viscosity zone and thin lithosphere, representative of West Antarctic regions. E5: Thli, very thick lithosphere, representative of East Antarctic regions. Identical viscosity values are offset slightly so that all vertical segments are visible.

Here we apply a fully coupled ice sheet and global Earth-sea level model to Antarctica to investigate the sensitivity of long-term variations to a range of five Earth viscoelastic profiles, during (1) the last deglacial retreat of the past ~20 kyr, (2) future warming under Intergovernmental Panel on Climate Change (IPCC) greenhouse-gas scenario Representative Concentration Pathway 8.5 (RCP8.5), and (3) the mid-Pliocene (~3 Ma). A large ensemble of deglacial simulations is performed, including five different viscoelastic Earth profiles, as a robust calibration of the coupled model. For the future and Pliocene simulations, only five runs are performed using the top-scoring sets of parameters in the deglacial ensemble for each Earth profile. The paper follows on from Gomez et al. (2015), who used the same coupled model in simpler future warming scenarios. Their results are discussed and compared with ours in sections 3 and 4.

In this paper, as in all those mentioned above, the Earth model is limited to 1-D radially varying viscoelastic profiles, without lateral heterogeneity. This does not capture the pronounced lateral variations between East and West Antarctica and within the West Antarctic region inferred from seismic data (An et al., 2015; Heeszel et al., 2016; Kaufmann et al., 2005; Morelli & Danesi, 2004; d. Nield et al., 2012). One of our vertical

profiles does have a very low viscosity zone in the upper mantle and thin lithosphere (LVZ, Low Viscosity Zone, labeled E4 below) representative of West Antarctica, but this is applied globally. Work is in progress to enable laterally heterogeneous structure in our Earth model (d. van der Wal et al., 2015).

2. Methods

The Antarctic ice sheet shelf model used here is described in detail in Pollard and DeConto (2012a), and additionally in Pollard et al. (2015) and DeConto and Pollard (2016). It uses a hybrid combination of Shallow Ice-Shallow Shelf Approximation (SIA-SSA) ice dynamics, which consider vertical shearing (SIA) and horizontal stretching (SSA) while neglecting higher-order modes of flow. A flux condition at the grounding line (Schoof, 2007) is imposed that allows reasonable grounding-line migration without very fine resolution in the grounding zone. These approximations yield satisfactory results in long-term large-scale intercomparisons versus higher-order models (Pattyn et al., 2012, 2013). The distribution of basal sliding coefficients under modern grounded regions is determined from a previous inverse run fitting to modern ice thicknesses (Pollard & DeConto, 2012b) and is assumed fixed in time. The model is run on a polar stereographic grid with 20 km grid resolution.

Climate forcing is obtained either from modern data sets with spatially uniform perturbations, or from Regional Climate Model simulations spanning Antarctica, as described in previous papers and outlined briefly below. Monthly mean air temperatures and precipitation are interpolated to the ice sheet grid and lapse rate corrected to the ice surface elevation (Pollard & DeConto, 2012a), and a simple model is used to estimate net surface mass balance using Positive Degree-Day melting and refreezing (similar to Robinson et al., 2010). Oceanic melting below floating ice shelves depends on the 400 m water temperature at the nearest ocean grid cell (Pollard & DeConto, 2012a; Pollard et al., 2015; see supporting information). This simple parameterization is used in several other long-term ice sheet studies; modeling ocean circulation under ice cavities with changing geometries is challenging and is left to future work (e.g., Seroussi et al., 2017).

The global Earth-sea level model and its coupling to the ice sheet model is as described in Gomez et al. (2013, 2015). The Earth-sea level model's physics include viscoelastic deformation of the solid Earth, Earth rotational effects, gravitational self-consistency leading to distortions in the position of the sea surface, and migrating shorelines. The ice margins in contact with the ocean fully respond to the evolving sea surface and solid Earth surface heights in the coupled model. That is, at frequent intervals, the ice loading history is passed to the global Earth-sea level model, which updates bedrock elevations relative to the current local sea surface equipotential and passes them back to the ice model. The coupling interval is 50 years for Pliocene simulations where initial rates of change are faster. For the longer but more gradual last deglacial simulations and

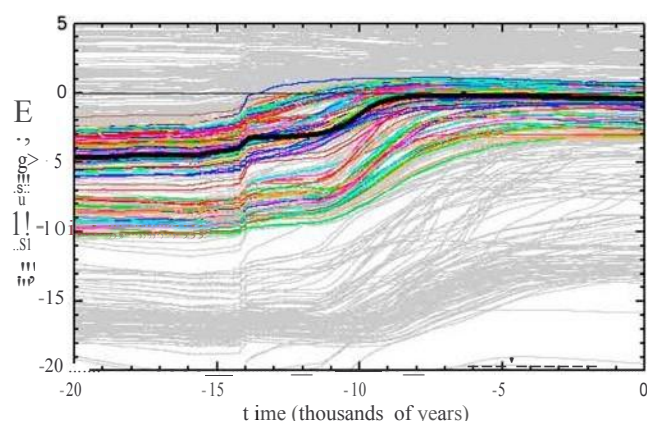


Figure 2. Contribution of the Antarctic ice sheet to global mean sea level (GMSL) versus time. Curves are shown for all 625 members of the large ensemble of last deglacial simulations. Time runs left to right, from 20,000 years before present to 0 (present). GMSL is calculated from the total Antarctic ice over flotation corresponding to current sea level and bedrock topography as the simulation evolves, divided by global ocean area, and relative to the value for the modern observed ice sheet (Bedmap2; Fretwell et al., 2013). Gray curves show runs whose scores are equal to or very close to 0 (very unrealistic). Colored curves are for the 120 better scoring runs, in descending-score order with 20 curves per color (red, orange, yellow, green, cyan, and blue). The thick black curve shows the best scoring run of the whole ensemble (OCFAC = 1, CALV = 0.7, SHELF = 10⁻⁵, EARTH = 4).

future extensions, that would result in prohibitive computer run times, and an interval of 200 years is used; shorter tests show that 50 versus 200 years makes very little difference to the results (see supporting information).

Model: Last Deglacial Retreat

As described in Gomez et al. (2013), the Earth model needs to be initialized to a near-equilibrated ice Earth state, as it is based on departures from initial equilibrium. Therefore each deglacial run is started at 40,000 years B.P. (before present; 40 ka), with the initial state of the Antarctic ice sheet provided by a previous run (see below). Deglacial simulations are run from 40 ka to 0 ka (modern), but only the last 20 kyr spanning the last deglacial retreat are analyzed, with the first 20 kyr regarded as spin-up. An "outer" iteration is performed in which departures of modern bedrock elevations from observed are used to correct the initial 40 ka bedrock elevation for the next iteration (Gomez et al., 2013; Kendall et al., 2005); this is done globally within the Earth-sea level model, and under Antarctica at the ice model resolution using Bedmap2 (Fretwell et al., 2013). The model is then rerun from 40 ka to 0 ka and the process is repeated. After four such iterations, departures from observed modern bedrock elevations are reduced to small levels (see Figure 8). The last outer iteration is used for the deglacial results analyzed below.



Figure 3. Scores for the complete large-ensemble suite of last deglacial simulations. All 625 runs are shown (four model parameters and five values each). The score values are computed versus geologic and modern data sets, normalized by the best score in the ensemble, and range from 0 (white, no skill) to 1 (bright red, best score). The figure is organized to show the scores in the 4-D space of parameter variations. The four model parameters, OCFAC, CALV, SHELF, and EARTH are described briefly in the text; the first three parameters, and the algorithms used to score each run versus data, are discussed in more detail in Pollard et al. (2016). Since each parameter only takes five values, the results are blocky but effectively show the behavior of the score over wide ranges of parameter values.

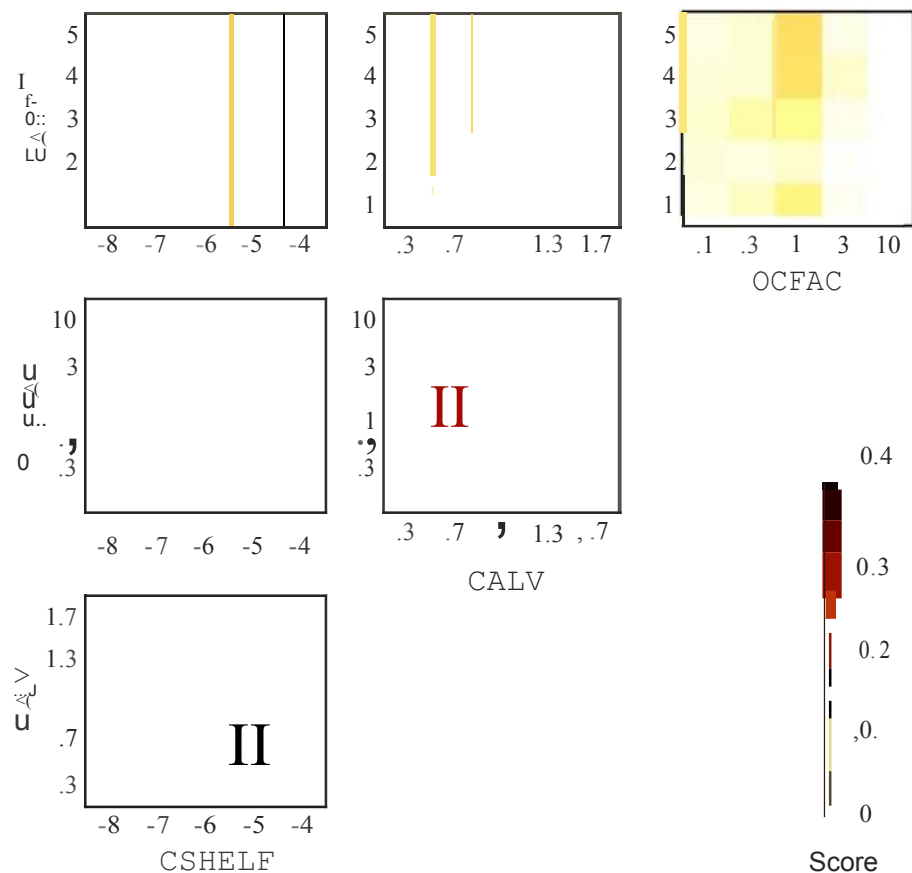


Figure 4. Mean scores for pairs of model parameters in the large ensemble of last deglacial simulations. These are the average scores for all runs with a given pair of parameter values, normalized so the sum for each pair is 1. The color scale saturates for scores of 0.4 and above (black).

The initial conditions at 40 ka are provided by a previous much longer glacial cycle run, with the same model except with coarser 40 km resolution and with an ELRA bed. The initial state at 40 ka is not critical for the results, as long as it is reasonably realistic and close to ice-bedrock equilibrium, because (1) its bedrock is adjusted by the outer iterations described above and (2) its ice distribution has little effect on later results after the spin-up period from 40 ka to 20 ka.

A large ensemble (LE) of 625 simulations from 40 ka to Oka is performed. An aggregate score (0 to 1) is computed for each run versus various geologic and modern data sets, and overall results are analyzed simply by taking ensemble-wide means weighted by the scores. The LE, scoring algorithms, and data sets are described in detail in Pollard et al. (2016). The data sets used are reconstructed past grounding-line locations, relative sea level records, cosmogenic elevation-age data, modern uplift rates, and modern ice distributions. Model misfits are averaged and combined into one score for each simulation using Gaussian error distribution concepts (Briggs & Tarasov, 2013; Pollard et al., 2016). In this study, a new parameter representing different viscoelastic Earth profiles is used in the LE to explore the sensitivity of the results to this input. The four model parameters varied in the ensemble, each taking five values, are

OCFAC = ocean melt factor, multiplying the standard ocean melt rate at the base of floating ice shelves (0.1, 0.3, 1, 3, 10).

CALV = calving coefficient, affecting the rate of iceberg calving (0.3, 0.7, 1, 1.3, 1.7).

CSHELF = basal sliding coefficient for modern oceanic (continental shelf) areas (10^{-8} , 10^{-7} , 10^{-6} , 10^{-5} , 10^{-4} m-a⁻¹ Pa⁻²).

EARTH = five different vertical viscoelastic profiles in the Earth model (E1 to E5).

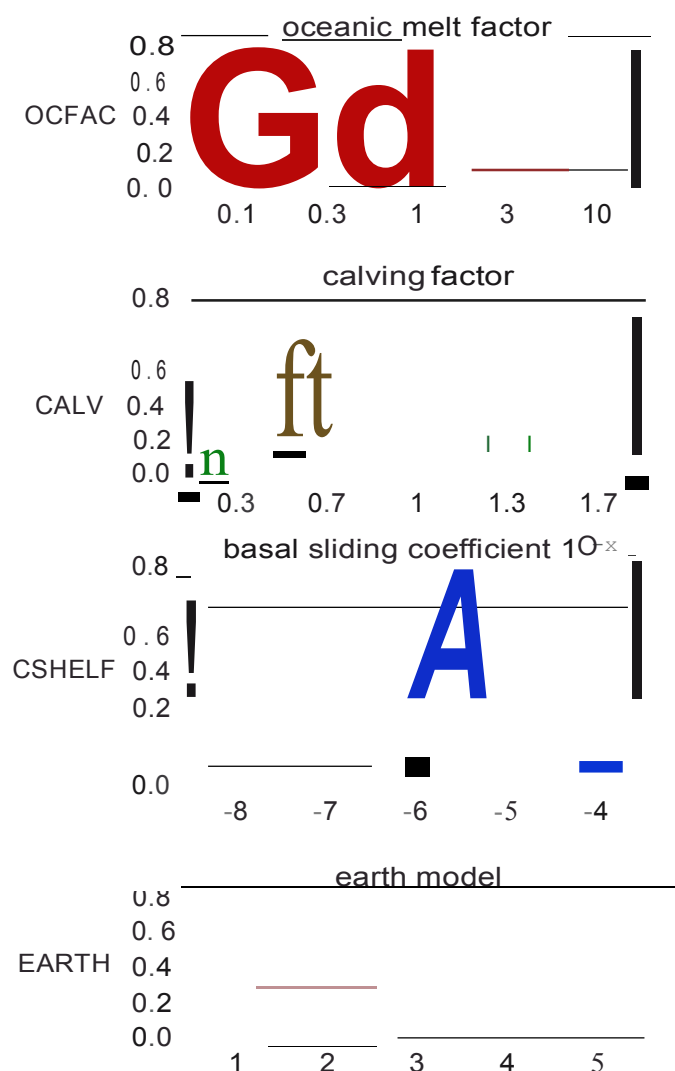


Figure 5. Mean scores for single model parameters in the large ensemble of last deglacial simulations. These are the average scores for all runs with a given single parameter value, normalized so the sum for each parameter is 1. The red triangle shows the mean of the parameter values weighted by the average scores shown, and whiskers show the 1-sigma standard deviations.

All possible combinations of these parameters are tested in the LE, requiring 625 (=5¹) runs. OCFAC, CALV, and (SHELF are described in more detail in Pollard et al. (2016). The five viscoelastic profiles for EARTH, E1 to E5, are shown in Figure 1, and numerical values are given in the supporting information. E1 (also labeled "HV" for "High Viscosity" and used in Gomez et al., 2013, 2015) is representative of a broad class of globally tuned Earth models favored by two independent groups (Lambeck et al., 1998, 2014; Mitrovica & Forte, 2004; LM in Raymo et al., 2011); we refer to E1 as the "standard" profile in presenting results

below. E4 (also labeled "LVZ" for "Low Viscosity Zone" and used in Gomez et al. 2015) is representative of West Antarctic regions, with a thin lithosphere of 50 km underlain by an additional very low viscosity zone of 10¹⁹ Pa s down to a depth of 200 km, and relatively low upper mantle viscosity below that. E3 (also labeled 50-p2-3) is similar to E4 but without the uppermost very low viscosity zone. E5 (also labeled Thli) has a much thicker lithosphere of 250 km and relatively high upper mantle viscosity and is representative of East Antarctic regions.

Although five Earth profiles are used in the large ensemble to provide a broad range for model calibration, it will be seen that subsequent results are quite similar for profiles E1, E2, and E5, and markedly different for E4, with E3 being intermediate between them. Consequently the

later discussions focus just on E1 ("HV," globally representative) and E4 ("LVZ," representative of West Antarctica).

As described in Pollard et al. (2016), atmospheric climate forcing is obtained from a modern Antarctic climatological data set (ALBMAP: Le Brocq et al., 2010), with simple uniform cooling perturbations proportional to a deep-sea core $\delta^{18}O$ stack (Lisiecki & Raymo, 2005). Subsurface oceanic temperatures are obtained from archived results of a global climate model simulation of the last 22 kyr (Liu et al., 2009). In the global Earth model, Northern Hemispheric ice loading history (outside the ice model domain) is prescribed from the ICE-SG data set (Peltier, 2004), which also influences circum-Antarctic sea levels felt by the ice model (see Figure 6).

Methods: Future

Future projections with the coupled model are obtained by continuing the last iteration of the deglacial runs for the next 5,000 years. As in DeConto and Pollard (2016), future atmospheric forcing is provided by a look-up table of previous atmospheric Regional Climate Model (RCM) simulations for specific CO₂ levels, interpolated appropriately for the CO₂ level at any time given by IPCC greenhouse-gas scenario RCP8.5 (business as usual), with CO₂ increasing to nearly 1,000 ppm by 2100 C.E. and nearly 2,000 ppm by 2300 C.E. (Meinshausen et al., 2011; van Vuuren et al., 2011). After 2500 C.E., we assume no further anthropogenic emissions and natural decay of CO₂ levels (Archer et al., 2009; DeConto & Pollard, 2016). Ocean temperatures at 400 m depth needed for the sub-ice shelf melt parameterization are prescribed from a transient National Center for Atmospheric Research Community Climate System Model version 4 global climate model simulation for RCP8.5 (Shields et al., 2016), as in DeConto and Pollard (2016). These future extensions are performed just for the best scoring run in the last deglacial LE for each Earth profile E1 to E5. We do not consider less extreme future emissions scenarios such as RCP2.6 and RCP4.5, in order to focus on the effects of Earth profiles with just one type of climate forcing for each time period. Gomez et al. (2015) show complementary results for less extreme future warming scenarios, as noted in section 4.

Two additional mechanisms are enabled for the future runs: hydrofracturing of ice shelves by surface melt,

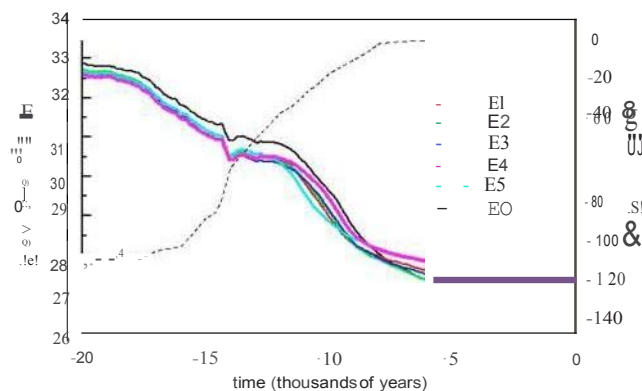


Figure 6. Total ice volume versus time before present for the last deglacial simulations. Only the bestscoring run in the large ensemble for each Earth viscoelastic profile E1 to E5 is shown. An earlier run using a simple ELRA bedrock model is also shown (EO), with asthenospheric e-folding relaxation time $\tau = 3$ kyr. The modern observed ice volume ($26.92 \times 10^6 \text{ km}^3$) is shown by an orange dot (Bedmap2; Fretwell et al., 2013). The dashed black line and right-hand axis show the global mean sea level equivalent of ice sheet variations in the ICE-SG data set (Peltier, 2004). Prescribed variations of northern hemispheric ICE-SG ice sheets influence geographically variable sea level variations in the Earth-sea level model, in addition to Antarctic variations from the coupled ice model. (The dashed line includes ICE-SG Antarctic contributions so does not exactly represent global sea level in our simulations).

where they would have negligible effects because the climates are colder than present (confirmed in simulations of the last 40 kyr, not shown).

2.3. Methods : Mid- Pliocene

Simulations for the mid-Pliocene representing a warm period around 3 Ma are performed with the bestscoring runs for Earth profiles E1 to E5. As in the future simulations, hydrofracturing and cliff failure processes are active, which produce collapse of both West and East Antarctic marine basins and -15 m rise in GMSL (global mean sea level) (Pollard et al., 2015). This is in better agreement with geologic records of mid-Pliocene shorelines, bearing in mind considerable uncertainties due to dynamic topography and Glacial Isostatic Adjustment (GIA) (Austermann et al., 2015; Raymo et al., 2011; Rovere et al., 2014; Rowley et al., 2013).

As described in Pollard et al. (2015), Pliocene atmospheric forcing is obtained from a Regional Climate Model (RCM) simulation with a CO_2 level of 400 ppm and an orbital configuration producing warm austral summers. Ocean temperatures are obtained from modern climatology (Levitus et al., 2012) and a prescribed uniform 2°C warming, broadly consistent with circum-Antarctic warming in Pliocene paleo-oceanic reconstructions (Dowsett et al., 2009).

The warm Pliocene simulations are initialized to "modern equilibrated" states and run for 10,000 years with invariant Pliocene

climate. These initial states are first obtained by extending the last iteration of the deglacial runs for 15,000 additional years with invariant modern climate, which allows remaining Glacial Isostatic Adjustments (GIAs) of the modern Antarctic bed to fully relax to equilibrium. We expect similar ice retreat to that in our future RCP8.5 (business as usual) simulations, because the combination of Pliocene orbital change and 400 ppm CO_2 produces a similar magnitude of Antarctic summer warming as future CC_i levels in the RCP85 scenario (DeConto & Pollard, 2016).

3. Results

3.1. Results: Last Deglacial Retreat

Figure 2 shows time series of the contribution of the Antarctic ice sheet to GMSL for the whole LE. The cloud of curves is similar to Figure 5 of Pollard et al. (2016), which used an ELRA bedrock model. The net contribution to GMSL rise from Last Glacial Maximum to modern is -3 to 8 m for the higher-scoring runs in Figure 2b, somewhat smaller than in other recent studies using ice sheet models (Briggs et al., 2013; Golledge et al., 2013; Maris et al., 2015; Whitehouse, Bentley, and Le Brocq, 2012; Whitehouse, Bentley, Milne, et al., 2012). This difference is mostly due to high continental-shelf basal sliding coefficients (CSHELF), producing thinner West Antarctic ice (seen also in Figure 3).

Figures 3-5 show mean scores for all parameter combinations (Figure 3), pairs of parameter values (Figure 4), and single parameter values (Figure 5). These figures show that the scores depend relatively little on EARTH, that is, for any one of the five Earth profiles (E1 to E5), reasonably realistic simulations can be obtained by appropriate choices of the other parameters. In comparison, the full range of other model parameters such as OCFAC and CSHELF produces a wider range of results from realistic to very unrealistic. Analogous behavior was seen in a similar large ensemble using a simple ELRA bedrock model, with the same model parameter variations as here except with EARTH replaced by the ELRA asthenospheric e-folding time (Pollard et al., 2016). The probability distribution functions and best fit values of OCFAC, CALV, and (SHELF) are reasonably similar to the earlier results. We note that the range of continental-shelf basal sliding coefficients, CSHELF, is wider here than in Pollard et al. (2016). Figure 5c shows that there is a pronounced maximum in the scores at $-1.0 \times 10^{-5} \text{ m a}^{-1} \text{ Pa}^{-2}$, confirming the expectation that extremely slippery values of 1.0×10^{-4} and above may not be realistic.

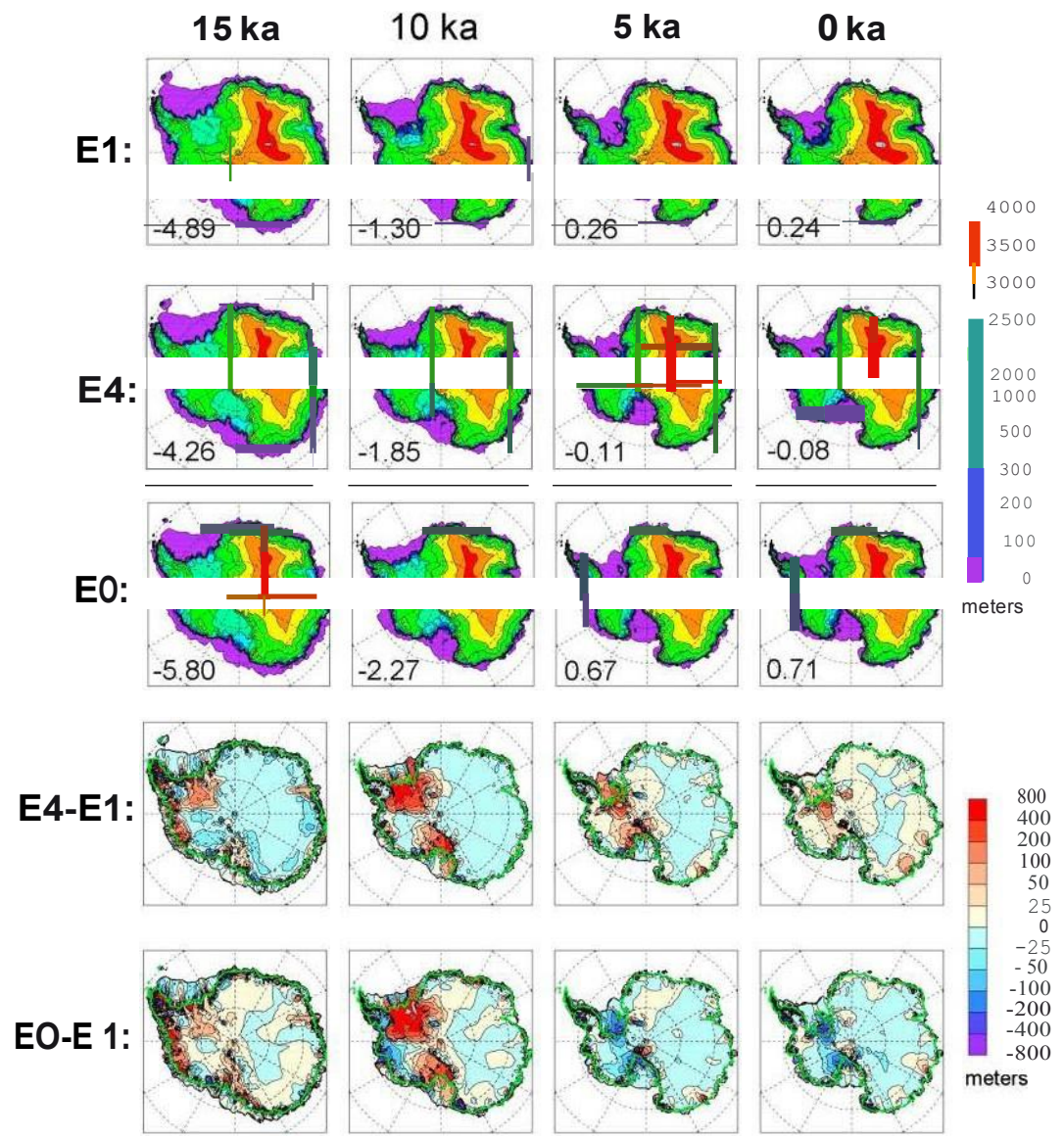


Figure 7. Snapshots at given times in last deglacial simulations shown in Figure 6. *E1*: Ice surface elevations for the run with the standard *E1* Earth viscoelastic profile (typical of Earth profiles adopted in some previous global ice age studies). The lowest elevation bin (purple) corresponds closely to floating ice shelves, and its inner border corresponds closely to the grounding line. *E4*: with the *E4* Earth profile (very weak upper mantle zone, thin lithosphere). *EO*: with a simple ELRA bedrock model and $\tau = 3$ kyr. The value in each panel is the contribution to global mean sea level (meters), relative to the modern observed icesheet (Bedmap2; Fretwell et al., 2013). *E4-E1*: Differences in ice thickness (*E4* - *E1*). *EO-E1*: Differences in ice thickness (*EO* - *E1*). In the difference panels, the *E4* or *EO* grounding line is shown by a thick green line.

Notably, the asthenospheric e-folding time in Pollard et al. (2016) is the LE parameter with the least effect on scores, as is EARTH here. The reason for this insensitivity is presumably the relatively slow time scales of deglacial retreat compared to the more rapid retreat seen in the future and Pliocene experiments, as discussed further below. This is due to the different time scales of the climatic forcing, and also the different geographical regions traversed by the grounding lines, with reversesloping beds accelerating future and Pliocene retreat.

Figure 6 shows time series of total ice volume of the best scoring run for each of the five Earth profiles, along with an earlier run using an ELRA bedrock model. The values of the three other parameters in the ensemble and in the ELRA run are all the same: OCFAC = 1, CALV = 0.7, and (SHELF = 10^{-5} (as seen in Figure 3).

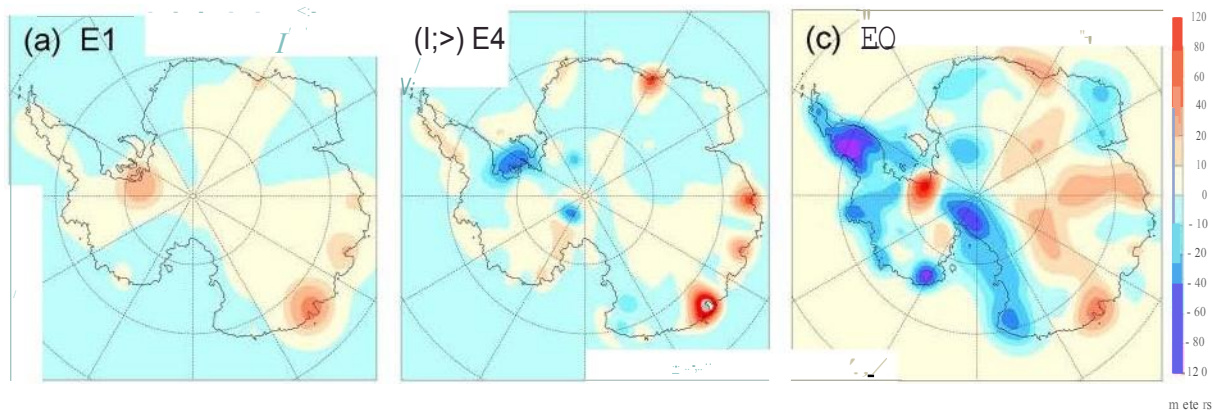


Figure 8. Differences in modern bedrock elevation from observed (Fretwell et al., 2013) at the end of the three deglacial simulations in Figure 7. **E1**: with standard Earth viscoelastic profile. **E4**: with E4 Earth profile (very weak upper mantle zone, thin lithosphere). **EO**: with a simple ELRA bedrock model and $-r = 3$ kyr.

Differences between the curves are quite small. For E4 (very weak upper mantle zone, thin lithosphere), ice volumes in the later phases of retreat are slightly greater than the other runs. This is expected because of greater negative feedback with E4 associated with rapidly rebounding bedrock as ice margins retreat, producing shallower grounding-line depths and reduced ice flux from the interior (Adhikari et al., 2014; Gomez et al., 2013, 2015; Konrad et al., 2015). As an overall measure of the effect of Earth profiles in the last deglacial retreat, the ratio of the maximum ice volume difference between E1 and E4 at any time during the runs, relative to the E1 change from 20 ka to 0 ka, is 8%.

Figure 7 shows snapshots of ice elevations for the best scoring runs with the standard "HV" profile E1 and "LVZ" profile E4, and for an earlier run with the ELRA bedrock model. As expected from the small differences in Figure 6, the grounding-line extents and large-scale ice thicknesses are generally similar between the runs. However, on regional scales and at particular time intervals there are significant differences, notably in West Antarctic Ross and Weddell embayments around 10 ka, where the stronger negative feedback with E4 reduces ice drawdown and preserves thicker ice compared to E1.

Figure 8 shows departures from modern observed bedrock elevations, at the end of the best fit runs for profiles E1 and E4 (after four outer iterations), and for the ELRA model run EO. As expected, the departures are considerably less for E1 and E4 than with the ELRA model, because no iteration is performed with the latter model to converge to the observed modern bed. For E1 and E4, the convergence is not complete, and bulls-eye errors still exist in several marginal regions. The departures for E1 are noticeably smaller than for E4, suggesting either that the E1 profile may be a better overall average for Antarctica, or simply that the more localized deformations and greater feedbacks with E4 require more iterations to converge. In any case, a more preferable approach in future work will be to use spatially heterogeneous Earth profiles, as discussed below.

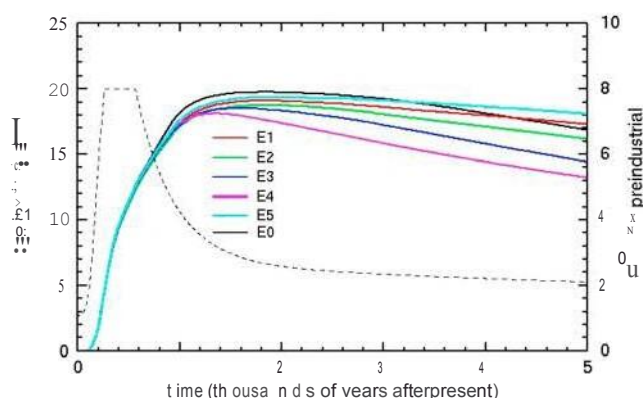


Figure 9. Contribution of the Antarctic ice sheet to global mean sea level rise relative to the model's present state, versus time after "present" (0 year, corresponding to 1950 C.E.), in future simulations with greenhouse-gas scenario RCP8.5. **E1 to E5**: for the five Earth viscoelastic profiles in this study. **EO**: with a simple ELRA bedrock model and $-r = 3$ kyr. The dashed black line and right-hand axis show the prescribed equivalent atmospheric CO₂ amount relative to preindustrial (280 ppm), following RCP8.5 to 2300 C.E., constant from 2300 to 2500 C.E., and decaying naturally with no anthropogenic emissions thereafter, as in DeConto and Pollard (2016).

3.2. Results: Future

Figure 9 shows time series of the contribution of the Antarctic ice sheet to global mean sea level rise for 5,000 years into the future. Relatively large differences begin to emerge after ~1,000 model years, especially for the two Earth profiles E3 and E4 (see Figure 1) with thin lithospheres and low viscosities in the upper mantle. The E4 profile (very weak upper mantle zone, thin lithosphere) produces the least retreat and 4 m less sea level rise than E1 after 5,000 years, much as in Gomez et al. (2015) who compared E1 versus E4 profiles using simpler climate warming.

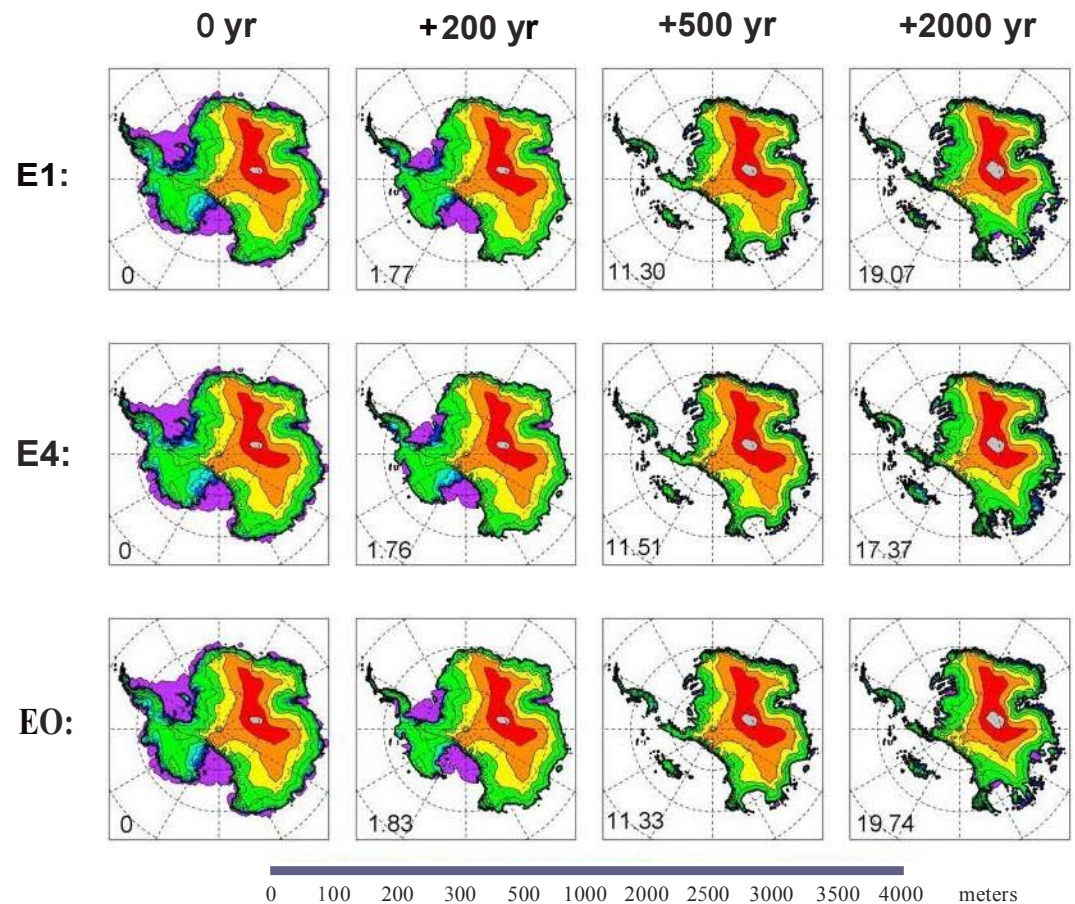


Figure 10. Snapshots of ice surface elevation at given times after present in future RCP8.5 simulations. The lowest elevation bin (purple) corresponds closely to floating ice shelves. The value in each panel shows the contribution to global mean sea level (meters), relative to the model's present state at 0 year. E1: with the standard Earth viscoelastic profile. E4: with E4 Earth profile (very weak upper mantle zone, thin lithosphere). EO: with a simple ELRA bedrock model and $\tau = 3$ kyr.

This is due to greater negative feedback on grounding-line retreat in E3 and E4 produced by more rapidly rebounding bedrock elevations in retreating marine basins, as described above and in Gomez et al. (2015). Most of the difference between E1 and E4 occurs after $\sim 1,000$ years and is due to retreat in major East Antarctic basins; however, this result is questionable because the E4 profile is not appropriate for those regions, as discussed further in section 4.

As discussed above, the runs here include two newly proposed mechanisms that cause drastic marine ice collapse in warmer climates: hydrofracturing of ice shelves by surface melt, and structural collapse of tall ice cliffs (DeConto & Pollard, 2016; Pollard et al., 2015). These mechanisms, combined with the strong climate warming in RCP8.5, cause very rapid collapse of West Antarctica in the first few hundred years, which overwhelms the influence of Earth profiles so that all curves in Figure 9 are nearly the same during this period, and begin to diverge only after ~ 700 years when East Antarctic retreat becomes significant (which occurs well after WAIS collapse because the EAIS basins are protected by narrower and shallower sills (Pollard et al., 2015)). Much the same insensitivity to Earth structure is also seen in the first few hundred years of Gomez et al.'s (2015) simulations, even in their milder warming cases (two times and four times preindustrial CO_2) and without the new mechanisms. Because of the slower retreat rates, their runs tend to diverge at an earlier stage than ours, when grounding lines are still retreating across West Antarctica; this indicates that Earth structure may still play an important role in early West Antarctic retreat for some greenhouse scenarios, as discussed in section 4.

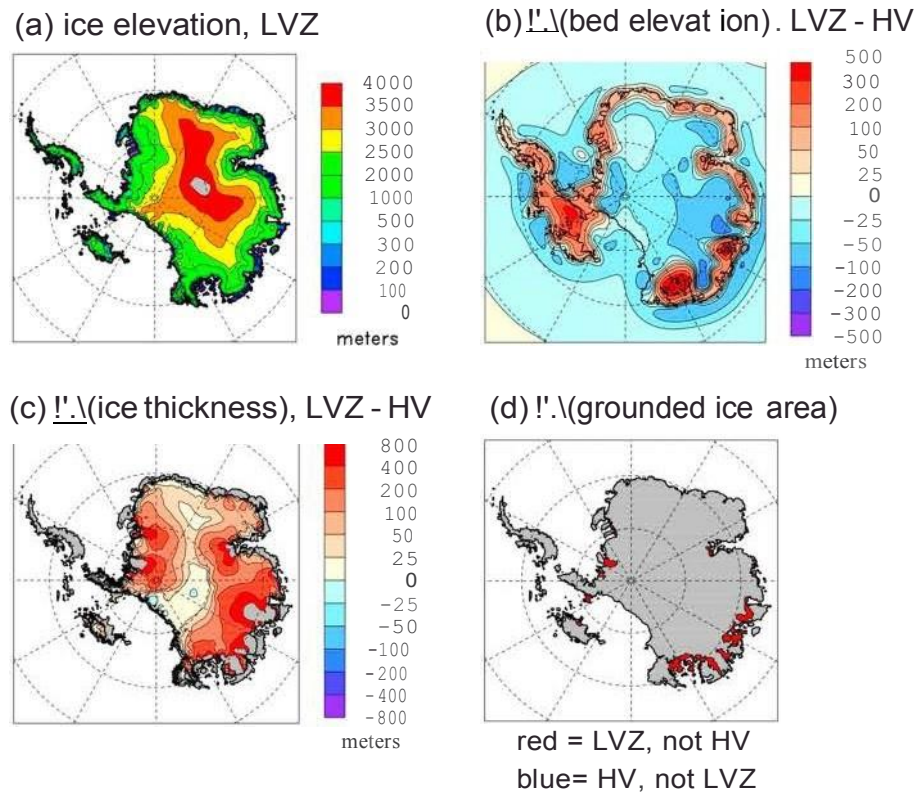


Figure 11. Quantities at 3,000 years after present in future RCPS.5 simulations, for Earth viscoelastic profiles E1 (standard) versus E4 (very weak upper mantle zone, thin lithosphere). (a) Ice surface elevations for E4. (b) Difference in bedrock elevations, E4 - E1. (c) Difference in ice thickness, E4 - E1. (d) Difference in grounded ice area. Red shows areas with grounded ice in E4 and no grounded ice in E1, and vice versa for blue (which does not occur).

In the later parts of the runs, the slow decline in equivalent sea levels is due to the assumed post-RCP85 natural decay of atmospheric CO₂, which allows the ice sheet to begin along-term recovery (DeConto & Pollard, 2016). In both the midretreat and regrowth phases, the stronger negative feedbacks with E3 and E4 reduce sea level rise compared to those with the other Earth profiles. As an overall measure, the ratio of the maximum sea level difference between E1 and E4 at any time during the runs, relative to the E1 sea level rise from 0 to 5 ka, is 23%.

Selected snapshots of ice elevations are shown in Figure 10 for the E1 and E4 profiles, and for an analogous future run with an ELRA bedrock model (EO). The largest differences in grounding-line extent occur later in the major Wilkes and Aurora basins of East Antarctica, where the stronger negative feedback of E4 causes significantly less grounding-line retreat into the basin interiors.

Figure 11 illustrates the mechanisms involved in the negative feedback, showing differences between the E4 and E1 runs at 3,000 years into the future (when GMSL rise is still near maximum but after significant differences in GMSL have emerged in Figure 9). The simulation with E4 has higher bedrock elevations and thus shallower bathymetry around much of the retreating Antarctic periphery (Figure 11b), which allows less ice flux across the grounding line (Schoof, 2007), and so preserves greater grounded ice thicknesses in upstream regions (Figure 11c) with slightly less grounding-line recession (Figure 11d). Similar results are found in Gomez et al. (2015), discussed further in section 4.

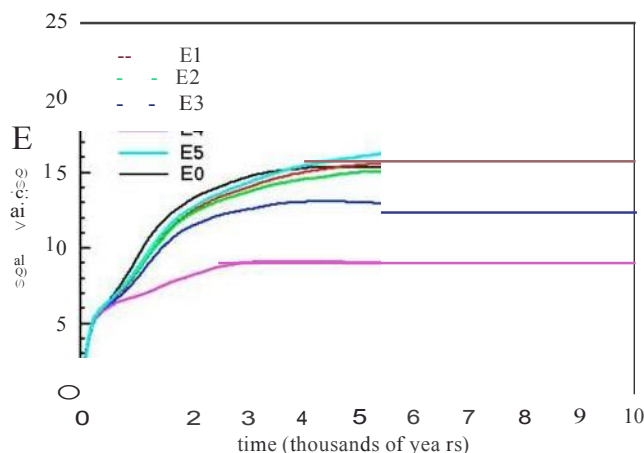


Figure 12. Contribution of the Antarctic ice sheet to global mean sea level versus time, relative to the model's state at 0 years, after a stepfunction change to warm mid-Pliocene climate. E1 to E5: for the five Earth viscoelastic profiles in this study. EO: with a simple ELRA bedrock model and $\tau = 3$ kyr.

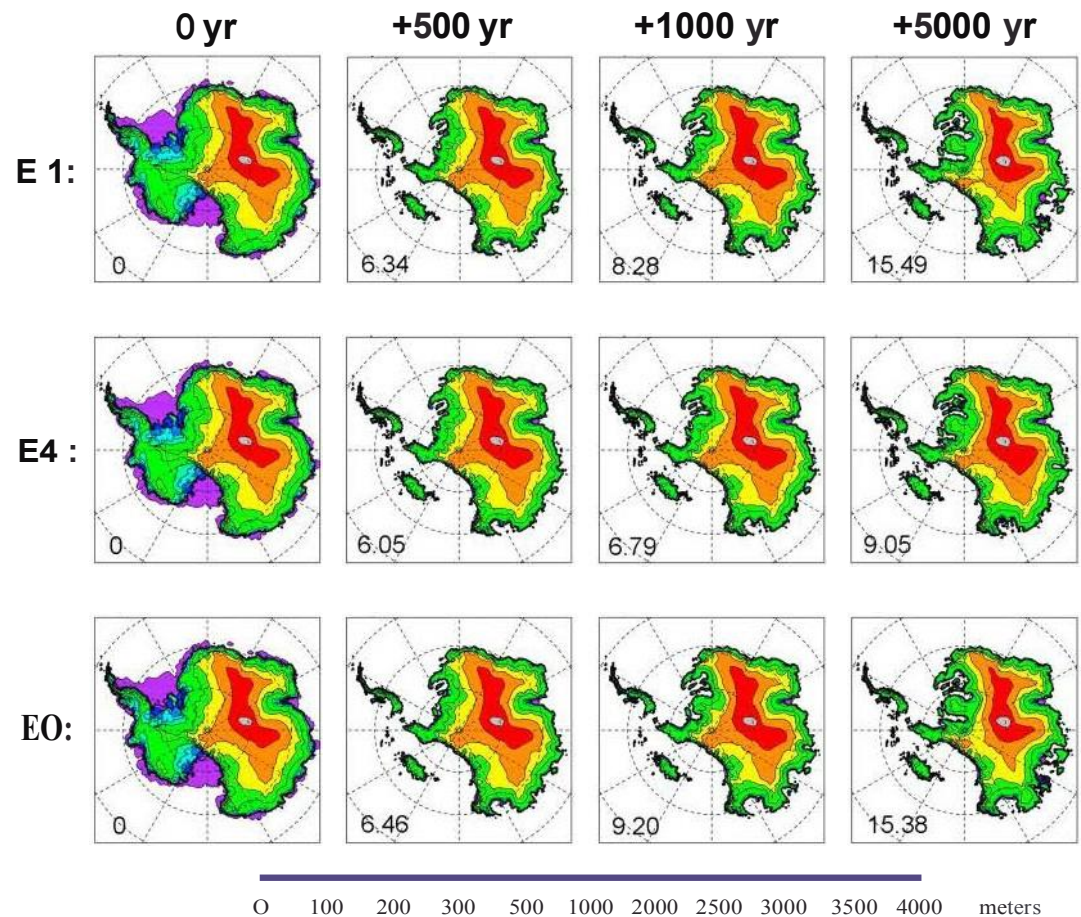


Figure 13. Snapshots of ice surface elevation at given times after a step function change from modern to warm mid-Pliocene (~ 3 Ma) climate. The lowest elevation bin (purple) corresponds closely to floating ice shelves. The value in each panel shows the contribution to global mean sea level (meters), relative to the model's state at 0 year. *E1*: with the standard Earth viscoelastic profile. *E4*: with *E4* Earth profile (very weak upper mantle, thin lithosphere). *EO*: with a simple ELRA bedrock model and $\tau = 3$ kyr.

3.3. Results: Mid-Pliocene

Figure 12 shows time series of the contribution of the Antarctic ice sheet to global average sea level rise for Earth profiles E1 to E5, along with an earlier run with an ELRA bed (EO), after a step function change to warm mid-Pliocene climate. The two Earth profiles E3 and E4 with thin lithospheres and low viscosities in the upper mantle produce much less sea level rise than the other profiles. As in the future simulations above, this is due to greater negative feedback in E3 and E4 produced by more rapidly rebounding bedrock elevations and localization of deformation to the grounding line in retreating marine basins. Because the climate perturbation is sustained in the Pliocene runs, there is no gradual ice regrowth and long-term decline in sea levels as in the future simulations (Figure 9). As an overall measure, the ratio of the maximum sea level difference between E1 and E4 at any time during the runs, relative to the E1 sea level rise from 0 to 10 ka, is 43%.

As in the future simulations, snapshots of ice surface elevations for E1, E4, and EO in Figure 13 show that the differences in retreat with E4 are located mainly in the Wilkes and Aurora basins of East Antarctica; implications are discussed in section 4. Ice retreat into these basins occurs later and more slowly in the Pliocene simulations (~ 1 to 3 kyr into the run) compared to the future RCP 8.5 simulations (0.4 to 15 kyr), due to differences in the climate forcing. The longer time scale of EAIS basin retreat in the Pliocene is intermediate between the time scales of bedrock rebound for E4 versus E1, amplifying the difference in their feedbacks on ice retreat, and producing a greater reduction in sea level rise (E4 compared to E1 in Figure 12 versus Figure 9). However, this conclusion depends on the form of the climate forcing and could change if more

realistic orbitally driven, time-continuous forcing is used in Pliocene simulations, which we plan to pursue in further work.

4. Conclusions

The radial profile of Earth viscosity can have significant effects on ice sheet variations during rapid retreat scenarios examined here, on time scales of several hundred to a few thousand years. Profiles with relatively weak upper mantles and thin lithospheres (labeled E3 and E4 here) produce a significant reduction in ice retreat for future and warm-Pliocene climate scenarios. The largest effects are seen for the E4 profile with a very weak upper mantle zone representative of West Antarctic regions. As discussed above, the reduction in ice loss compared to that with the standard EI profile is due to greater and more rapid rebound of bedrock under the retreating ice near the grounding lines of marine basins, producing shallower grounding-line depths and less ice flux from upstream grounded ice (Gomez et al., 2015). For deglacial retreat of the past ~20 kyr, the climate forcing and ice retreat is more gradual, and the results with E3 and E4 are more similar to those with the other Earth profiles.

This study follows on from Gomez et al. (2015), who used the same coupled ice and Earth-sea level model as here, except that our ice model includes two newly developed ice sheet retreat mechanisms—hydrofracturing and ice cliff failure (DeConto & Pollard, 2016; Pollard et al., 2015). Gomez et al. (2015) considered a range of climate warming scenarios but with a simpler treatment in which atmospheric CO₂ was ramped up linearly to a single level (two times, four times, or eight times preindustrial). Their results focused on comparing two Earth profiles—HV (our EI) and LVZ (our E4)—and they found that LVZ reduces ice retreat significantly compared to HV on hundreds of year time scales, somewhat shorter than in this study due to the added mechanisms accelerating ice sheet retreat here. For 8xCO₂ warming, more comparable to the RCP8.5 scenario used here, their final HV versus LVZ differences in East Antarctica dominate over West, consistent with our results. However, Gomez et al. (2015) found that for relatively mild warming (2xCO₂, not considered here), differences between HV and LVZ can be large in West Antarctica, both early and late in the retreat. This may indicate that Earth model properties will be important in future West Antarctic response if warming follows less extreme RCP2.6 or RCP4.5 scenarios.

As noted above, many studies have assessed Antarctic GIA models versus deglacial data, driven by uncoupled ice loading histories. In particular, Whitehouse, Bentley, Milne, et al. (2012) show large misfits between model and observed relative sea level (RSL) data, for a wide range of lithospheric thickness and upper and lower mantle viscosities. As seen above, all five of our viscoelastic profiles EI to ES produce good scores versus deglacial data including RSL. Two of our profiles (EI and E2) have properties within Whitehouse et al.'s ranges of good fits (their Figure 4), but the other three (E3, E4, and ES) lie far outside their good fit ranges. Part of this discrepancy is likely due to physical differences between the Earth and ice sheet models, but it could also be due to the wider ranges of other model parameters explored in our large ensemble.

Results using a simple ELRA bedrock model (EO) are similar to those with the standard Earth sea level model (EI, with stronger upper mantle and thicker lithosphere), as shown in Figures 6, 9, 12, and other figures. This indicates that the overall results of our previous long-term studies with an ELRA model are not overly dependent on the type of bedrock model, with the exception of low-viscosity-layer/thin lithosphere Earth profiles as described above. We also note that the choice of Earth profile or model (among all those used here including ELRA) has little impact in the first few hundred years of future RCP8.5 simulations (Figure 9), during which rapid West Antarctic collapse produced by hydrofracturing and ice cliff failure overwhelms Earth ice feedbacks. However, beyond overall large-scale ice sheet behavior, coupling with Earth-sea level models is needed to capture other important features such as sea level gravitational effects, regional bed response, forebulges, and lateral Earth variations.

The results presented here focus on large-scale differences in ice loading history and the overall contribution of Antarctic ice to GMSL rise. The impact of varying Earth model parameters on sea level and surface deformation in particular geographic regions may be considerable. Consideration of the time scale, forcing, and region of interest of a given problem is needed in order to select an appropriate radially varying Earth structure to capture the feedback between solid Earth deformation on Antarctic ice sheet evolution. It may not be appropriate to apply a single radially varying Earth model to simulate changes across the whole of Antarctica.

as done here, motivating the consideration of lateral variations in Earth structure in future work. The vertical viscoelastic profiles in the Earth model considered here are laterally homogeneous, and some of the above conclusions could change when more realistic laterally varying profiles are used. For instance, in the future and Pliocene runs with the E4 profile, most of the difference in retreat lies in major basins of East Antarctica, for which the E4 profile is clearly not realistic. Furthermore, recent data analyses (e.g., Heeszel et al., 2016) have found that upper mantle viscosities under localized regions of West Antarctica may be even lower than in our E4 profile. Work to enable laterally heterogeneous viscoelastic properties in our Earth model is underway.

Acknowledgments

We thank Johannes Sutter and two anonymous reviewers for their careful and helpful reviews. This work was supported by National Science Foundation grants OCE-1202632 (PUOMAX), DMS-1418090, GEO-1240507, and OPP-1341394 and by National Oceanic and Atmospheric Administration grant NA13OAR4310100. N.G. is funded by the Natural Science and Engineering Research Council, the Canada Research Chairs program, the Canadian Foundation for Innovation and McGill University. Selected output files, metadata, and ice sheet model code are available at Penn State's Data Commons <http://www.datacommons.psu.edu>, <https://doi.org/10.18113/D3SS9W>.

References

- Adhikari, S., Ivins, E.R., & Larour, E. (2016). ISSM-SESAM v1.0: Mesh-based computation of gravitationally consistent sea-level and geodetic signatures caused by cryosphere and climate driven mass change. *Geoscientific Model Development*, 9, 1087-1109. <https://doi.org/10.5194/gmd-9-1087-2016>
- Adhikari, S., Ivins, E.R., Larour, E., Seroussi, H., Morlighem, M., & Nowicki, S. (2014). Future Antarctic bed topography and its implications for ice sheet dynamics. *Solid Earth*, 5, 569-584. <https://doi.org/10.5194/se-5-569-2014>
- An, M., Wiens, D.A., Zhao, Y., Feng, M., Nyblade, A.A., Kanao, M., ... Leveque, J.J. (2015). S-velocity model Antarctic Plate from Rayleigh waves. *Journal of Geophysical Research: Solid Earth*, 120, 359-383. <https://doi.org/10.1002/2014JB011332>
- Archer, D., Eby, M., Brovkin, V., Ridgwell, A., Cao, L., Mikolajewicz, U., ... Tokos, K. (2009). Atmospheric lifetime of fossil fuel carbon dioxide. *Annual Review of Earth and Planetary Sciences*, 37, 117-134. <https://doi.org/10.1146/annurev.earth.031208.100206>
- Austermann, J., Pollard, D., Mitrovica, J., X. Moucha, R., Forte, A.M., DeConto, R.M., ... Raymo, M.E. (2015). The impact of dynamic topography change on Antarctic ice sheet stability during the mid-Pliocene warm period. *Geology*, 43, 927-930. <https://doi.org/10.1130/G36988.1>
- Briggs, R.D., Pollard, D., & Tarasov, L. (2013). A glacial systems model configured for large ensemble analysis of Antarctic deglaciation. *The Cryosphere*, 7, 1949-1970. <https://doi.org/10.5194/tc-7-1949-2013>
- Briggs, R.D., & Tarasov, L. (2013). How to evaluate model-derived deglaciation chronologies: A case study using Antarctica. *Quaternary Science Reviews*, 63, 109-127. <https://doi.org/10.1016/j.quascirev.2012.11.021>
- Bueler, E., Lingle, C.S., & Brown, J. (2007). Fast computation of a viscoelastic deformable Earth model for ice-sheet simulations. *Annals of Glaciology*, 46, 97-105. <https://doi.org/10.3189/172756407782871567>
- de Boer, S., Stocchi, P., & van de Wal, R.S.W. (2014). A fully coupled 3-D ice-sheet sea-level model: Algorithm and applications. *Geoscientific Model Development*, 7, 2141-2156. <https://doi.org/10.5194/gmd-7-2141-2014>
- de Boer, S., Dolan, A.M., Bernales, J., Gasson, E., Goelzer, H., Gollledge, N.R., ... van de Wal, R.S.W. (2015). Simulating the Antarctic ice sheet in the late-Pliocene warm period: PLISMIP ANT, an ice-sheet model intercomparison. *The Cryosphere*, 9, 881-903. <https://doi.org/10.5194/tc-9-881-2015>
- de Boer, S., Stocchi, P., Whitehouse, P.L., & van de Wal, R.S.W. (2017). Current state and future perspectives on coupled ice-sheet-sea-level modeling. *Quaternary Science Reviews*, 169, 13-28. <https://doi.org/10.1016/j.quascirev.2017.05.013>
- DeConto, R.M., & Pollard, D. (2016). Contribution of Antarctica to past and future sea-level rise. *Nature*, 531, 591-597. <https://doi.org/10.1038/nature17145>
- Dowsett, H.J., Robinson, M.M., & Foley, K.M. (2009). Pliocene three-dimensional global ocean temperature reconstruction. *Climate of the Past*, 5, 769-783. <https://doi.org/10.5194/cp-5-769-2009>
- Dziewonski, A.M., & Anderson, D.L. (1981). Preliminary reference Earth model (PREM). *Physics of the Earth and Planetary Interiors*, 25(4), 297-356. [https://doi.org/10.1016/0031-9201\(81\)9004-6](https://doi.org/10.1016/0031-9201(81)9004-6)
- Feldmann, J., & Levermann, A. (2015). Collapse of the West Antarctic Ice Sheet after local destabilization of the Amundsen Basin. *Proceedings of the National Academy of Sciences of the United States of America*, 112, 14, 191-194, 196. <https://doi.org/10.1073/pnas.1512482112>
- Fretwell, P., Pritchard, H.D., Vaughan, D.G., Bamber, J., L. Barrand, N., Bell, R., ... Zirizzotti, A. (2013). Bedmap2: Improved ice bed, surface and thickness datasets for Antarctica. *The Cryosphere*, 7, 375-393. <https://doi.org/10.5194/tc-7-375-2013>
- Gollledge, N.R., L. Cowlwowski, D.E., Naish, T.R., Levy, R.H., Fogwill, C.J., & Gasson, E.G.W. (2015). The multi-millennial Antarctic commitment to future sea-level rise. *Nature*, 526, 421-425. <https://doi.org/10.1038/nature15706>
- Gollledge, N.R., Levy, R.H., McKay, R.M., Fogwill, C.J., White, D.A., Graham, A.G.C., ... Hall, B.L. (2013). Glaciological and geological signature of the Last Glacial Maximum Antarctic ice sheet. *Quaternary Science Reviews*, 78, 225-247. <https://doi.org/10.1016/j.quascirev.2013.08.011>
- Gomez, N., Pollard, D., & Holland, D. (2015). Sea level feedback lowers projections of future Antarctic ice sheet mass loss. *Nature Communications*, 6, 8798. <https://doi.org/10.1038/ncomms9798>
- Gomez, N., Pollard, D., & Mitrovica, J.X. (2013). A 3-D coupled ice sheet-sea level model applied to Antarctica through the last 40 ky. *Earth and Planetary Science Letters*, 384, 88-99. <https://doi.org/10.1016/j.epsl.2013.09.042>
- Heeszel, D., S. Wiens, D.A., Anandakrishnan, S., Aster, R.C., Dalziel, I.W.D., Huerta, A.D., ... Winberry, J.P. (2016). Upper mantle structure of central and West Antarctica from array analysis of Rayleigh wave phase velocities. *Journal of Geophysical Research: Solid Earth*, 121, 1758-1775. <https://doi.org/10.1002/2015JB012616>
- Kaufmann, G., Wu, P., & Ivins, E.R. (2005). Lateral viscosity variations beneath Antarctica and their implications on regional rebound motions and seismotectonics. *Journal of Geodynamics*, 39, 165-181. <https://doi.org/10.1016/j.jog.2004.08.009>
- Kendall, R.A., Mitrovica, J.X., & Milne, G.A. (2005). On post-glacial sea level-II. Numerical formulation and comparative results on spherically symmetric models. *Geophysical Journal International*, 161, 679-706. <https://doi.org/10.1111/j.1365-246X.2005.02553.x>
- Konrad, H., Sasgen, I., Pollard, D., & Klemann, V. (2015). Potential of the solid-Earth response for limiting long-term West Antarctic Ice Sheet retreat in a warming climate. *Earth and Planetary Science Letters*, 432, 254-264. <https://doi.org/10.1016/j.epsl.2015.10.008>
- Lambeck, K., Rouby, H., Purcell, A., Sun, Y., & Sambridge, M. (2014). Sea-level and global ice volumes from the Last Glacial Maximum to the Holocene. *Proceedings of the National Academy of Sciences of the United States of America*, 111, 15, 296-15,303. <https://doi.org/10.1073/pnas.1411762111>
- Lambeck, K., Smither, C., & Johnston, P. (1998). Sea-level change, glacial rebound and mantle viscosity for northern Europe. *Geophysical Journal International*, 134(1), 102-144. <https://doi.org/10.1046/j.1365-246X.1998.00541.x>

- Le Brocq, A. M., Payne, A. J., & Vieli, A. (2010). An improved Antarctic dataset for high resolution numerical ice sheet models (ALBMAP v1). *Earth System Science Data*, 2, 247-260. <https://doi.org/10.5194/essd-2-247-2010>
- Le Meur, E., & Huybrechts, P. (1996). A comparison of different ways of dealing with isostasy: Examples from modelling the Antarctic ice sheet during the last glacial cycle. *Annals of Glaciology*, 23, 309-317. <https://doi.org/10.3183/AGU20030500013586>
- Levitus, S., Antonov, J. I., Boyer, T. P., Baranova, O. K., Garcia, H. E., Locarni, R. A., ... Zweng, M. M. (2012). World ocean heat content and thermocline sea level change (0-2000 m), 1955-2010. *Geophysical Research Letters*, 39(10), L10603. <https://doi.org/10.1029/2012GL051106>
- Lingle, C. S., & Clark, J. A. (1985). A numerical model of interactions between a marine ice sheet and the solid Earth: Application to a West Antarctic ice stream. *Journal of Geophysical Research*, 90(1), 1100-1114. <https://doi.org/10.1029/JC090i01p01100>
- Lisiec, L. E., & Raymo, M. E. (2005). Pleistocene stack of 57 globally distributed benthic foraminiferal records. *Paleoceanography*, 20, PA1003. <https://doi.org/10.1029/2004PA001071>
- Liu, Z., Otto-Bliesner, B. L., He, F., Brady, E. C., Tomas, R., Clark, P. U., ... Cheng, J. (2009). Transient simulation of last deglaciation with a new mechanism for Bolling-Allerod warming. *Science*, 325, 310-314. (Extended to modern: www.cgd.ucar.edu/ccr/TraCE), 5938. <https://doi.org/10.1126/science.1171041>
- Maris, M. N. A., van Wessem, J. M., van de Berg, W. J., de Boer, B., & Oerlemans, J. (2015). A model study of the effect of climate and sea-level change on the evolution of the Antarctic ice sheet from the Last Glacial Maximum to 2100. *Climatic Change*, 127, 837-851. <https://doi.org/10.1007/s00381-014-2317-z>
- Martin, M. A., Winkelmann, R., Haseloff, M., Albrecht, T., Bueler, E., Khroulev, C., & Levermann, A. (2011). The Potsdam Parallel Ice Sheet Model (PISM-PIK) - Part 2: Dynamic equilibrium simulation of the Antarctic ice sheet. *The Cryosphere*, 5, 727-740. <https://doi.org/10.5194/tc-5-727-2011>
- Meinshausen, M., Smith, S. J., Calvin, K., Daniel, J. S., Kainuma, M. L. T., Lamarque, J.-F., ... van Wren, D. P. (2011). The RCP greenhouse gas concentrations and their extensions from 1765 to 2300. *Climatic Change*, 109, 213-241. <https://doi.org/10.1007/s10584-011-0156-z>
- Mercer, J. H. (1978). West Antarctic ice sheet and CO₂ greenhouse effect: A threat of disaster. *Nature*, 271, 321-325. <https://doi.org/10.1038/271321a0>
- Mitrovica, J. X., & Forte, A. M. (2004). A new inference of mantle viscosity based upon joint inversion of convection and glacial isostatic adjustment data. *Earth and Planetary Science Letters*, 225, 177-189. <https://doi.org/10.1016/j.epsl.2004.06.005>
- Morelli, A., & Danesi, S. (2004). Seismological imaging of the Antarctic continental lithosphere: A review. *Global and Planetary Change*, 42, 155-165. <https://doi.org/10.1016/j.gloplacha.2003.12.005>
- Nield, G. A., Whitehouse, P. L., King, M. A., Clarke, P. J., & Bentley, M. J. (2012). Increased ice loading in the Antarctic Peninsula since the 1850s and its effect on glacial isostatic adjustment. *Geophysical Research Letters*, 39(17), L17504. <https://doi.org/10.1029/2012GL052559>
- Pattyn, F. (2017). Sea-level response to melting of Antarctic ice shelves on multi-centennial timescales with the fast Elementary Thermomechanical Ice Sheet model (ETISH v1.0). *The Cryosphere*, 11, 1851-1878. <https://doi.org/10.5194/tc-11-1851-2017>
- Pattyn, F., Perichon, L., Durand, G., Favier, L., Gagliardini, O., Hindmarsh, R. C. A., ... Wilkens, N. (2013). Grounding-line migration in plan-view marine ice sheet models: Results of the ice2sea MISIP3d intercomparison. *Journal of Glaciology*, 59, 410-422. <https://doi.org/10.3189/2013JG12J129>
- Pattyn, F., Schoof, C., Perichon, L., Hindmarsh, R. C. A., Bueler, E., de Fleurian, B., ... Vieli, A. (2012). Results of the marine ice sheet model intercomparison project, MISIP. *The Cryosphere*, 6, 573-588. <https://doi.org/10.5194/tc-6-573-2012>
- Peltier, W. R. (2004). Global glacial isostasy and the surface of the ice-age Earth: The ICE-5G (VM2) model and GRACE. 2004. *Annual Review of Earth and Planetary Sciences*, 32, 111-149. <https://doi.org/10.1146/annurev.earth.32.082503.144359>
- Pollard, D., & DeConto, R. M. (2012a). Description of a hybrid ice sheet-shelf model, and application to Antarctica. *Geoscientific Model Development*, 5, 1273-1295. <https://doi.org/10.5194/gmd-5-1273-2012>
- Pollard, D., & DeConto, R. M. (2012b). A simple inverse method for the distribution of basal sliding coefficients under ice sheets, applied to Antarctica. *The Cryosphere*, 6, 953-971. <https://doi.org/10.5194/tc-6-953-2012>
- Pollard, D., DeConto, R. M., & Alley, R. B. (2015). Potential Antarctic ice sheet retreat driven by hydrofracturing and ice cliff failure. *Earth and Planetary Science Letters*, 412, 112-121. <https://doi.org/10.1016/j.epsl.2014.12.035>
- Pollard, D., Chang, W., Haran, M., Applegate, P., & DeConto, R. (2016). Large ensemble modeling of last deglacial retreat of the West Antarctic ice sheet: Comparison of simple and advanced statistical techniques. *Geoscientific Model Development*, 9, 1697-1723. <https://doi.org/10.5194/gmd-9-1697-2016>
- Raymo, M. E., Mitrovica, J. X., O'Leary, M. J., DeConto, R. M., & Hearty, P. J. (2011). Departures from eustasy in Pliocene sea-level records. *Nature Geoscience*, 4, 328-332. <https://doi.org/10.1038/ngeo1118>
- Robinson, A., Calov, R., & Ganopolski, A. (2010). An efficient regional energy-moisture balance model for simulation of the Greenland ice sheet response to climate change. *The Cryosphere*, 4, 129-144. <https://doi.org/10.5194/tc-4-129-2010>
- Rovere, A., Raymo, M. E., Mitrovica, J. X., Hearty, P. J., O'Leary, M. J., & Inglis, J. D. (2014). The Mid-Pliocene sea-level conundrum: Glacial isostasy, eustasy and dynamic topography. *Earth and Planetary Science Letters*, 387, 27-33. <https://doi.org/10.1016/j.epsl.2013.10.030>
- Rowley, D. B., Forte, A. M., Moucha, R., Mitrovica, J. X., Simmons, N. A., & Grand, S. P. (2013). Dynamic topography change of the eastern United States since 3 million years ago. *Science*, 340, 1560-1563. <https://doi.org/10.1126/science.1229180>
- Schoof, C. (2007). Ice sheet grounding line dynamics: Steady states, stability, and hysteresis. *Journal of Geophysical Research*, 112, F03S28. <https://doi.org/10.1029/2006JF000664>
- Seroussi, H., Nakayama, Y., Larour, E., Menemenlis, D., Morlighem, M., Rignot, E., & Khazendar, A. (2017). Continued retreat of Thwaites Glacier, West Antarctica, controlled by bed topography and ocean circulation. *Geophysical Research Letters*, 44, 6191-6199. <https://doi.org/10.1002/2017GL072910>
- Shields, C. A., Kiehl, J. T., & Meehl, G. A. (2016). Future changes in regional precipitation simulated by a half-degree coupled climate model: Sensitivity to horizontal resolution. *Journal of Advances in Modeling Earth Systems*, 8, 863-884. <https://doi.org/10.1002/2015MS000884>
- Stocchi, P., Escutia, C., Houben, A. J. P., Vermeersen, B. L. A., Bijl, P. K., Brinkhuis, H., ... IODP Expedition 318 scientists (2013). Relative sea-level rise around East Antarctica during Oligocene glaciation. *Nature Geoscience*, 6, 380-384. <https://doi.org/10.1038/ng01783>
- Tarasov, L., & Peltier, W. R. (2004). A geophysically constrained large ensemble analysis of the deglacial history of the North American ice-sheet complex. *Quaternary Science Reviews*, 23, 359-388. <https://doi.org/10.1016/j.quasdev.2003.08.004>
- van der Wal, W., Whitehouse, P. L., & Schrama, E. J. O. (2015). Effect of GIA models with 30 composite mantle viscosity on GRACE mass balance estimates for Antarctica. *Earth and Planetary Science Letters*, 414, 134-143.
- van Vuuren, D. P., Edmonds, J., Kainuma, M., Riahi, K., Thomson, A., Hibbard, K., & Rose, S. K. (2011). The representative concentration pathways: An overview. *Climatic Change*, 109, 5-31. <https://doi.org/10.1007/s10584-011-0148-z>

- Weertman, J. (1974). Stability of the junction of an ice sheet and an ice shelf. *Journal of Glaciology*, 13(6,7) 3-11. <https://doi.org/10.3189/50022143000023327>
- Whitehouse, P. L., Bentley, M. J., & Le Brocq, A. M. (2012). A deglacial model for Antarctica: Geological constraints and glaciological modeling as a basis for a new model of Antarctic glacial isostatic adjustment. *Quaternary Science Research*, 32 1-24. <https://doi.org/10.1016/j.quascirev.2011.11.016>
- Whitehouse, P. L., Bentley, M. J., Milne, G. A., King, M. A., & Thomas, I. D. (2012). A new glacial isostatic model for Antarctica: Calibrated and tested using observations of relative sea-level change and present-day uplifts. *Geophysical Journal International*, 190 1464-1482. <https://doi.org/10.1111/j.1365-246X.2012.05557.x>